Macromolecules

Article

pubs.acs.org/Macromolecules

Effect of Oxygen Inhibition on the Kinetic Constants of the UV-Radical Photopolymerization of Diurethane Dimethacrylate/Photoinitiator Systems

Kentaro Taki,*[,†] Yoshihito Watanabe,[‡] Hiroshi Ito,[§] and Masahiro Ohshima[‡]

[†]Department of Mechanical Systems Engineering, Yamagata University, 4-3-16, Jonan, Yonezawa, Yamagata, 992-8510, Japan

[‡]Department of Chemical Engineering, Kyoto University, Katsura, Nishikyoku, Kyoto, 615-8510, Japan

[§]Department of Polymer Science and Engineering, Yamagata University, 4-3-16, Jonan, Yonezawa, Yamagata, 992-8510, Japan

ABSTRACT: The kinetic constants of propagation (k_p) and termination (k_t) for a diurethane dimethacrylate/1-hydroxycyclohexyl phenyl ketone (Irgacure 184) system were measured using a dark polymerization technique that employs real-time FT-IR spectroscopy to measure the conversion and reaction rate of the methacrylate group at different time points. The sample was placed between two optically polished KBr plates with a 10 μm metal spacer. A series of measurements resulted in a gradual peak in the kinetic constants at a 0.15 conversion of the methacrylate group. The kinetic constants for the conversion, which ranged from 0.15 to 0.5, were used to obtain the parameters of the Anseth−Bowman model to generate a numerical simulation of the photopolymerization kinetics. The kinetic equations, the oxygen inhibition reaction-diffusion equation, and the macroradical mass balance model indicated that the gradual peak in the kinetic constant was caused by an oxygen inhibition reaction. The Anseth−Bowman model for k_p and k_t was effective even if oxygen inhibition occurred, when the oxygen inhibition reaction−diffusion equation was employed.

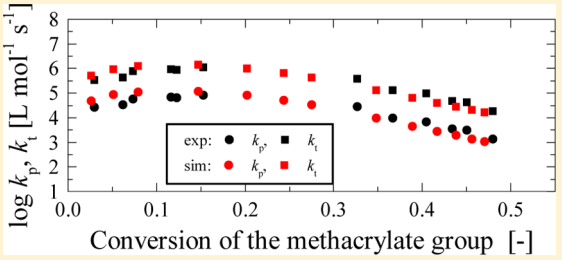

INTRODUCTION

Photoinduced curing, where curing refers to the irreversible transformation of a liquid polymerizable formulation into a stable solid, has advanced greatly over the last half century.[1−7] UV curing represents the majority of radiation curing methods, which also include UV and electron beam curing. It is used in a wide range of applications both in traditional and high-tech industries, including laser imaging, microlithography, stereolithography, microelectronics, optics, holography, medicine, and nanotechnology.[3]

Although photocuring has a wide range of applications, most acrylated materials undergo radical polymerization and are thus intrinsically vulnerable to inhibition by molecular oxygen, resulting in incomplete curing, which is manifested particularly by a tacky upper surface or, in extreme cases, by a complete failure to cure.[4] Because open-air curing is, in the majority of cases, the simplest method for industrial processing, oxygen inhibition is a common issue and is generally found in free radical photocuring applications.[4] Because of the tremendous industrial importance of photocuring, a wealth of scientific publications and patents on strategies to overcome oxygen inhibition have been published,[8] including a number of scientific reviews.[9−12] Ligon et al. thoroughly reviewed recent studies of oxygen inhibition and proposed several possible strategies, for both academic and industrial applications.[4]

Roll-to-roll UV nanoimprinting is a sophisticated technology for creating large patterned structures of cross-linked polymers on a substrate.[13−17] The nanostructured surface exhibits characteristic properties, including a unique structural color[14,15] and dewetting.[18] Although the continual advancement of mold fabrication technology is certain to allow an increased number of commercial applications for continuous roller imprinting, the cost of the nanostructured molds for the UV nanoimprinting process remains an issue. Indeed, to achieve the desired characteristics of a nanoimprinted product, the nanostructured mold must be modified by trial-and-error, thus increasing the total cost. Acrylic resins, which are sensitive to oxygen, are currently the most widely used resins because they are produced by fast radical polymerization and are suitable for high throughput applications.[17,19] Partially polymerized resins can cake onto the mold, making it necessary to clean or discard the mold, which greatly reduces throughput.[17] Oxygen inhibition is inconvenient for UV roller imprinting, in which vacuum processing is very difficult to implement due to its reliance on a continuous feedstock.[17]

Minimizing the number of trials to build the nanostructured mold requires computer-aided design software to model the UV-cured coatings of nanostructured molds. The numerical simulation of cure kinetics is an effective means to indirectly determine how monomers polymerize in the nanomold.

Because of the cross-linking nature of UV cure resins, their kinetics exhibit diffusion limitations even during the initial

Received: November 27, 2013
Revised: February 13, 2014
Published: March 6, 2014

Table 1. Reaction Scheme and Kinetic Model of the Photopolymerization

reaction scheme	kinetic model	equation number
	Dissociation of Photoinitiator by UV Irradiation	
$PI \xrightarrow{h\nu} 2I^{\bullet}$	$R_i = \phi\varepsilon[PI]I_0 \exp(-\varepsilon[PI]z)$	(1)
	$\frac{\partial[PI]}{\partial t} = -\frac{1}{2}R_i$	(2)
	Primary Radical Formation	
$I^{\bullet} + M \rightarrow I\text{-}M^{\bullet}$	$\frac{\partial[I^{\bullet}]}{\partial t} = R_i - k_i[I^{\bullet}][M]$	(3)
	Propagation Reaction	
$I\text{-}M_n^{\bullet} + M \xrightarrow{k_p} I\text{-}M_{n+1}^{\bullet}$	$\frac{\partial[M]}{\partial t} = -k_i[I^{\bullet}][M] - k_p[M][M_n^{\bullet}]$	(4)
	Bimolecular Termination	
$I\text{-}M_n^{\bullet} + I\text{-}M_n^{\bullet} \xrightarrow{k_t} I\text{-}M_nM_m\text{-}I$	$\frac{\partial[M_n^{\bullet}]}{\partial t} = k_i[I^{\bullet}][M] - k_t[M_n^{\bullet}]^2 - k_O[M_n^{\bullet}][O_2]$	(5)
	Oxygen Inhibition Reaction	
$I\text{-}M_n^{\bullet} + O_2 \xrightarrow{k_O} I\text{-}M_nOO^{\bullet}$	$\frac{\partial[O_2]}{\partial t} = D_O\frac{\partial^2[O_2]}{\partial z^2} - k_O[O_2][M_n^{\bullet}]$	(6)

stages of the reaction. Initially, the rate increases dramatically due to the diffusion-controlled termination process, which leads to autoacceleration. As the reaction progresses, the propagation reaction also becomes diffusion limited, and the polymerization rate decreases substantially, referred to as autodeceleration.[20,21] The diffusion of small species, such as initiators, monomers, primary radicals and oxygen molecules, and macro radicals is an important aspect of photoinduced cross-linking bulk polymerization; thus, mass transfer is critical.[1,6,22−25]

Complete kinetic models of photopolymerization describing nonuniform temperature distribution; the diffusion of monomers, radicals, and oxygen; and chain length dependent rates of propagation and termination have been developed during the past 25 years.[6,19,26−36]

There are three types of formulations that include the effects of the diffusion-controlled mass transfer of small species. The first involves a set of mass transfer (diffusion−reaction) equations.[6,19] The effect of mass transfer is explicitly incorporated into the diffusion terms of the mass transfer equation. The diffusion coefficients of the species decrease with increasing degrees of polymerization. The diffusion coefficients and kinetic constants are determined independently for the calculation.[6] Another formulation was proposed by Zhang et al. for the analysis of mobile and trapped radicals.[37] Finally, a third set of equations for the kinetic constants of propagation (k_p) and termination (k_t) as a function of the reaction ratio of the functional groups, i.e., the acrylated groups, is employed. Bowman and Peppas developed a model incorporating the strong relationship between the volume relaxation and the kinetics.[38] Anseth and Bowman developed equations for k_p and k_t as a function of the free volume fraction by incorporating the transition region for propagation and termination in terms of the resistance to reaction.[39] The other formulation developed by Kurdikar and Peppas employed the Vrentas−Duda relationship for the diffusion of small molecules in viscoelastic media.[40] A series of experimentally obtained kinetic constants was used to determine the parameters in the equations.

The free volume model describing changes in the kinetic constants of propagation and of bimolecular termination reactions upon conversion was proposed by Anseth and Bowman in 1993.[39] The model describes the decreases in the kinetic constants upon photopolymerization due to decreases in the free volume fraction. This model has been well examined for oxygen-free systems, as proven by experimental data for photopolymerization obtained using a thoroughly purged photo differential scanning calorimeter (photo DSC).[33,34,41]

However, the model has not yet been examined for oxygen-dissolved systems, in which oxygen from the air dissolves in a sample and inhibits photopolymerization as a view of kinetic constants. Most industrial processes occur under an air atmosphere, and oxygen inhibition cannot be avoided. Thus, this model is worth examining in conjunction with the reaction-diffusion equation of oxygen as the numerical simulation of cure kinetics becomes more convenient and efficient.

In this study, the effect of oxygen on the kinetic constants of propagation and termination was investigated. The dark polymerization method in conjunction with the real-time FT-IR spectroscopy was employed to measure propagation and termination constants. A theoretical model was then developed to generate a numerical simulation of the conversion of functional groups during dark simulation, where the mass balance equation of macroradicals was embedded in the model instead of the pseudo-steady-state approximation. The kinetic constants were obtained from the numerical simulation in the same manner that they were obtained from the experiment. Finally, the experimental result and simulation were compared to elucidate the effect of oxygen.

NUMERICAL SIMULATION OF THE PHOTOPOLYMERIZATION

Reaction Scheme and Mathematical Model. The oxygen inhibition of photoinduced radical polymerization consists of several steps.[42,43] First, oxygen can quench the excited state of the photoinitiator (PI). Second, it can react with primary initiating or propagating radicals to form peroxyl radicals, which are not energetically favorable for initiating acrylate polymerization. These peroxyl radicals terminate polymerization through radical−radical recombination or by abstracting hydrogen from an adjacent molecule, where the newly formed radical often has insufficient reactivity toward the acrylate double bond to reinstate the initiation process. A model of oxygen inhibition phenomena and photoinduced

dx.doi.org/10.1021/ma402437q | Macromolecules 2014, 47, 1906−1913

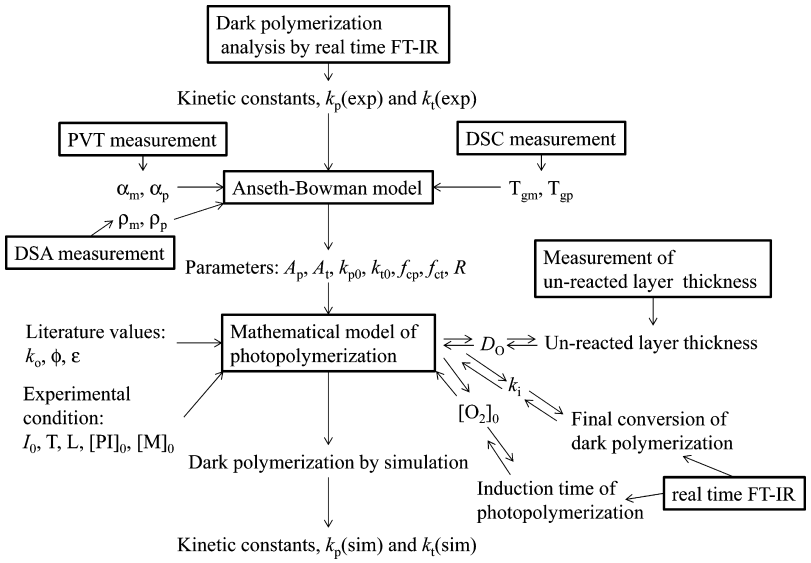

Figure 1. Flowchart to determine the parameters of the kinetic equations.

polymerization was summarized for the swollen polymer matrix by Krongauz, who conducted finite element computations of photopolymerization reaction kinetics under patterned illumination and without limitations, where all of the species besides the oligomers and the initiators were diffusive. Krongauz and co-workers investigated and modeled oxygen effects in the "patterned" photopolymerization encountered in the manufacturing of holographic gratings, photoresists and photolithographic imaging.[6] Furthermore, other studies have investigated primary radical mass balance, macroradical mass balance, and oxygen inhibition.[26,34,44−48] The photopolymerization reaction scheme considered in this study and the kinetic model that enabled the propagation, termination, dark polymerization, and oxygen inhibition reactions are shown in Table 1. In this study, the different molecular weight macroradicals were implicitly considered separately in the model because their kinetic parameters were difficult to determine consistently. The diffusion of the photoinitiator, monomer, and macroradical were not considered, unlike in previous studies, because our system was uniformly exposed to UV light and comprised an optically thin film; however, the diffusion of oxygen was considered. The diffusion coefficient of oxygen was considered constant because the reaction between oxygen and radicals reaches completion before vitrification begins. Moreover, it was assumed that the photopolymerization was isothermal.

The initial and boundary conditions for Table 1 are shown below.

Initial condition:

$$[PI]|_{t=0} = [PI]_0 \tag{7}$$

$$[I^\bullet]|_{t=0} = 0 \tag{8}$$

$$[M]|_{t=0} = [M]_0 \tag{9}$$

$$[M_n^\bullet]|_{t=0} = 0 \tag{10}$$

$$O_2|_{t=0} = [O_2]_0 \tag{11}$$

Boundary condition:

$$\left.\frac{\partial[X]}{\partial z}\right|_{z=0} = \left.\frac{\partial[X]}{\partial z}\right|_{z=L} = 0 \tag{12}$$

where ϕ is the quantum yield, ε is the molar absorption coefficient of the photoinitiator, $[PI]$ is the photoinitiator concentration, $[I^\bullet]$ is the photoinitiator radical concentration, I_0 is the light intensity, z is the position, k_i is the primary radical kinetic constant, k_p is the propagation reaction kinetic constant, $[M]$ is the monomer concentration, $[M_n^\bullet]$ is the macroradical concentration, k_t is the bimolecular termination kinetic constant, $[O_2]$ is the oxygen concentration, k_O is the oxygen inhibition reaction kinetic constant, and D_O is the diffusion coefficient of oxygen.

Because the UV-cured coating process involves bulk polymerization, vitrification occurs as the degree of polymerization increases. Vitrification slows the diffusion of monomers and reduces the reaction rates of both propagation and termination. The Anseth−Bowman model was employed to account for the decrease in the kinetic constant of the propagation and termination reactions as the conversion of the monomer increases.[39]

Propagation reaction kinetic constant:

$$k_p = k_{p0}(1 + \exp[-A_p(1/f - 1/f_{cp})])^{-1} \tag{13}$$

Termination reaction kinetic constant:

$$k_t = k_{t0}\left(1 + \frac{1}{\frac{Rk_p[M]}{k_{t0}} + \exp[-A_t(1/f - 1/f_{ct})]}\right)^{-1} \tag{14}$$

where k_{p0} and k_{t0} are the kinetic constants ideally determined without a vitrification effect. A_p and A_t are constants that control the rate at which the autoacceleration occurs. f is the free volume fraction, whereas f_{cp} and f_{ct} are the critical free volume fractions at which the reaction transitions from reaction-controlled to diffusion controlled propagation and termination. R is the constant of the reaction-diffusion transition.

The free volume fractions of both the monomer and polymer were calculated using the thermal expansion coefficient.

Free volume fraction of the monomer:

$$f_m = 0.025 + \alpha_m(T - T_{gm}) \tag{15}$$

dx.doi.org/10.1021/ma402437q | Macromolecules 2014, 47, 1906−1913

Free volume fraction of the polymer:

$$f_p = 0.025 + \alpha_p(T - T_{gp}) \tag{16}$$

Volume fraction of monomer as a function of the conversion of functional group:

$$\phi_m = \frac{1 - x}{1 - x + \frac{\rho_m}{\rho_p}x} \tag{17}$$

Linear relationship for the free volume fraction:

$$f = f_m\phi_m + f_p(1 - \phi_m) \tag{18}$$

where α_m and α_p are the thermal expansion coefficients of the monomer and polymer, respectively. T_{gm} and T_{gp} are the glass transition temperature of the monomer and polymer, respectively. ρ_m and ρ_p are the density of the monomer and polymer, respectively. x is the conversion of functional groups during the polymerization.

Flowchart of Parameter Determination. Determining the parameters in the above equations requires several steps, as shown in Figure 1. The kinetic constants were determined using the dark polymerization technique, which is explained later. The thermal expansion coefficient is determined using either the pressure−volume−temperature (PVT) measurement or the densitometry (DSA) of the polymer and monomer. The glass transition temperatures of the monomer and polymer are determined by differential scanning calorimetry (DSC). The kinetic constants, thermal expansion coefficients, density, and glass transition temperatures serve as the input of the Anseth−Bowman model to determine its parameters. In addition, the mathematical model of the photopolymerization described by eq 1 (in Table 1) to eq 18 uses the literature values and experimental conditions. The diffusion coefficient, initial concentration of oxygen, and primary radical kinetic constant (k_i) are then set to guessed values. The kinetic constant of the oxygen inhibition reaction (k_O) is set as 5×10^5 $m^3 \cdot mol^{-1} \cdot s^{-1}$ based on the literature.[26] The photopolymerization is then numerically simulated to determine the initial concentration of oxygen by trial and error to fit the induction time of the photopolymerization experimental data. The value of k_i at which the reaction had completed after the dark polymerization was determined by using trial-and-error. Finally, the diffusion coefficient of oxygen was determined using trial-and-error to fit the unreacted layer thickness from the experimental data. The measurement of the thickness of the unreacted layer has been reported elsewhere.[49] The boundary condition for oxygen described in eq 12 was then changed to the following equation:

$$[O_2]|_{z=0,t} = [O_2]|_0 \tag{19}$$

The diffusion of oxygen may in effect be negligible because of the thin sample used for the real-time FT-IR measurement.

Dark Polymerization Method. The well-established dark polymerization method was used to measure the kinetic constants as described previously.[5,41,50] First, the polymerization rate was monitored as a function of time, and the combined kinetic constant, $k_p/k_t^{1/2}$, was determined by steady-state analysis as follows:

$$\frac{k_p}{k_t^{1/2}} = \frac{R_p}{[M](\phi I_0 \varepsilon [PI])^{1/2}} \tag{20}$$

The rate of polymerization is represented by R_p. All other symbols are as previously described. The individual kinetic constants were then determined by monitoring the conversion in the dark and applying a nonsteady-state analysis after closing the shutter and terminating the radical initiation at various points during the reaction. The other combined kinetic constants described in eq 21, i.e., k_p/k_t and $k_t[M_n^\bullet]_{dark,0}$, were determined by fitting the equation to the experimental data for the dark polymerization:[49]

$$\ln \frac{[M]_{dark,0}}{[M]_{dark,t}} = \frac{k_p}{k_t}\ln(k_t[M_n^\bullet]_{dark,0}t + 1) \tag{21}$$

The terms $[M]_{dark,0}$ and $[M]_{dark,t}$ represent the molar concentrations of the methacrylate group in the monomer at the moment the shutter is closed and at an elapsed time t after closing the shutter, respectively. This analysis assumes that the kinetic constants do not change significantly with time.

MATERIALS AND METHODS

Materials. The difunctional UV curable monomer was diurethane dimethacrylate (DUDM, Aldrich). The photoinitiator was 1-hydroxycyclohexyl phenyl ketone (Irgacure 184, BASF). The weight ratio of Irgacure 184 to DUDM was 1:99. All materials were used as received. A bottle of KBr plates was supplied by JASCO (Japan). The KBr plates were polished with a piece of sandpaper, Colcothar/methanol slurry, and leather to achieve optically flat surface by a hand.

UV Light Source. Real-time FT-IR spectroscopy was used along with a UV light source (OmniCure S2000 High-Pressure 200-W Mercury-Vapor Short Arc lamp, EXFO, Mississaugua, Ontario, Canada) equipped with a liquid light guide (EXFO, Mississaugua, Ontario, Canada) to irradiate the monomer/initiator mixtures. The incident light intensity was monitored using a UV radiometer (UT-150, USHIO, Japan) with a maximum intensity of 365 nm prior to each characterization measurement.

Real-Time FT-IR Measurement. The pioneering use of real-time FT-IR to measure photoinduced polymerization was developed by Decker et al.[51] In this study, the measurement system was slightly modified to determine the onset time of UV light irradiation. Real-time FT-IR spectroscopy (VERTEX 70, Bruker Optics, Germany) was used to monitor the polymerization kinetics.[52] A schematic of the optical bench is illustrated in Figure 2. A horizontal-transmission accessory

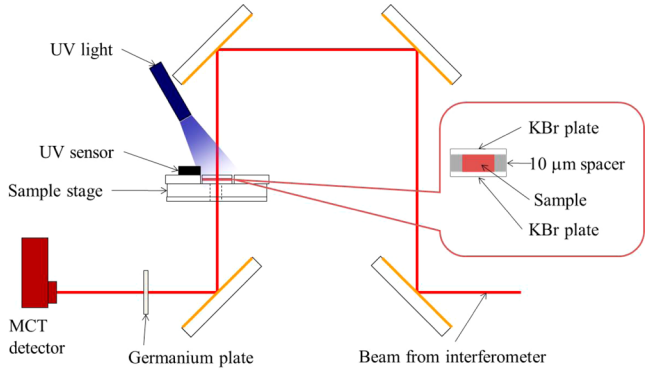

Figure 2. Optical bench of the real-time FT-IR measurement.

(HTA) was designed to enable the horizontal mounting of liquid samples for FT-IR measurements. A mercury cadmium telluride (MCT) detector and KBr-coated beam splitter combination was used in conjunction with the rapid-scan option of the spectrometer to obtain a temporal resolution (33 ms) sufficient for monitoring the photopolymerization. The UV light source was located 3 cm above the sample. The sample stage was maintained at 30 °C using a temperature-control device designed and constructed for use with a

dx.doi.org/10.1021/ma402437q | Macromolecules 2014, 47, 1906−1913

ceramic heater (Systems Engineering, Tokyo, Japan) in conjunction with the horizontal-transmission accessory. Samples (with a cured thickness of approximately 10 μm) were prepared by sandwiching a drop of the sample solution between two optically polished KBr plates (JASCO, Japan) with a 10 μm metal spacer (MISUMI, Japan). Each measured spectrum was processed using the peak-deconvolution software developed in our laboratory.[52]

The reaction rate constants of the propagation and termination reactions were determined using the dark polymerization analysis. The UV intensity was carefully adjusted by considering the absorbance of UV light by the KBr plate. The ON-OFF-timing of the UV light was precisely monitored and synchronized in front of the sample by a UV sensor.

RESULTS AND DISCUSSION

Figure 3 shows the kinetic constants of propagation (k_p) and termination (k_t) that were measured by real-time FT-IR and dark polymerization. When the conversion of the methacrylate group was less than 0.05, the k_p and k_t values were 10^4 and 10^5 L·mol^{-1}·s^{-1}), respectively. The values of k_p and k_t increased as the conversion proceeded, reaching a peak at 0.15 before decreasing. The solid line and the dotted line are the result of the fitting eqs 13 and eqs 14, respectively. These equations do not have a peak due to the mathematical shape of the function. Thus, the best fit was obtained between the conversions of 0.15 and 0.6. All determined parameters are provided in Table 2.

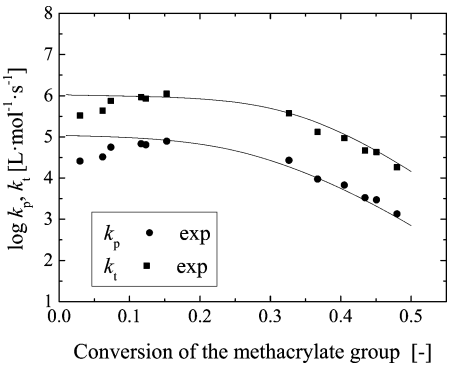

Figure 3. Experimental results for the determination of the kinetic constant and fitting of eqs 13 and 14

To further probe the mechanism responsible for the appearance of a peak at a conversion of 0.15, the photopolymerization was numerically simulated by setting the initial oxygen concentration to zero.

Figure 4 shows representative results for the experimental conversion of the methacrylate group and the numerical simulation of the oxygen-dissolved and oxygen-free systems. The UV intensity, I_0, was set to 10 mW·cm^{-2} at 0 s and 0 mW cm^{-2} at 3 s to numerically simulate the experimental

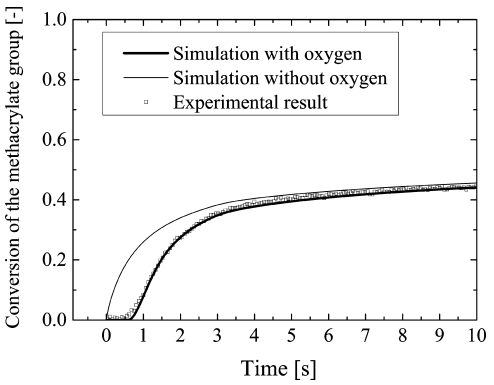

Figure 4. Conversion of the methacrylate group after 3 s UV irradiation. The results of the numerical simulation with and without oxygen are shown.

Table 2. Numerical Simulation Parameters of the Photopolymerization

parameter	value	units	source
ρ_m	1.103 459	kg·m^{-3}	measured
ρ_P	1.320	kg·m^{-3}	measured
α_m	5×10^{-4}	K^{-1}	measured
α_p	7.5×10^{-5}	K^{-1}	measured
T_{gm}	236.51	K	measured
T_{gP}	313.12	K	measured
A_p	1.26	–	fitted by nonlinear least-squares method
A_t	22.8	–	fitted by nonlinear least-squares method
k_{p0}	1.145×10^5	L·mol^{-1}·s^{-1}	fitted by nonlinear least-squares method
k_{t0}	1.337×10^6	L·mol^{-1}·s^{-1}	fitted by nonlinear least-squares method
f_{cp}	5.17×10^{-2}	–	fitted by nonlinear least-squares method
f_{ct}	5.81×10^{-2}	–	fitted by nonlinear least-squares method
R	11	–	
k_o	5×10^5	m^3·mol^{-1}·s^{-1}	Dendukuri, 2008[26]
ϕ	0.6	–	
ε	9.66×10^{-1}	m^3·mol^{-1}·m^{-1}	
I_0	10 (under the UV irradiation); 0 (without the UV irradiation)	mW·cm^{-2}	experimental condition
L	10×10^{-6}	m	experimental condition
T	303.15	K	experimental condition
$[PI]_0$	54.557	mol·m^{-3}	experimental condition
$[M]_0$	4.84×10^3	mol·m^{-3}	experimental condition
D_0	1.08×10^{-10}	m^2·s^{-1}	trial-and-error method
$[O_2]_0$	1.3×10^{-2}	mol·m^{-3}	trial-and-error method
k_i	4.8×10^{-5}	s^{-1}	trial-and-error method

dx.doi.org/10.1021/ma402437q | Macromolecules 2014, 47, 1906−1913

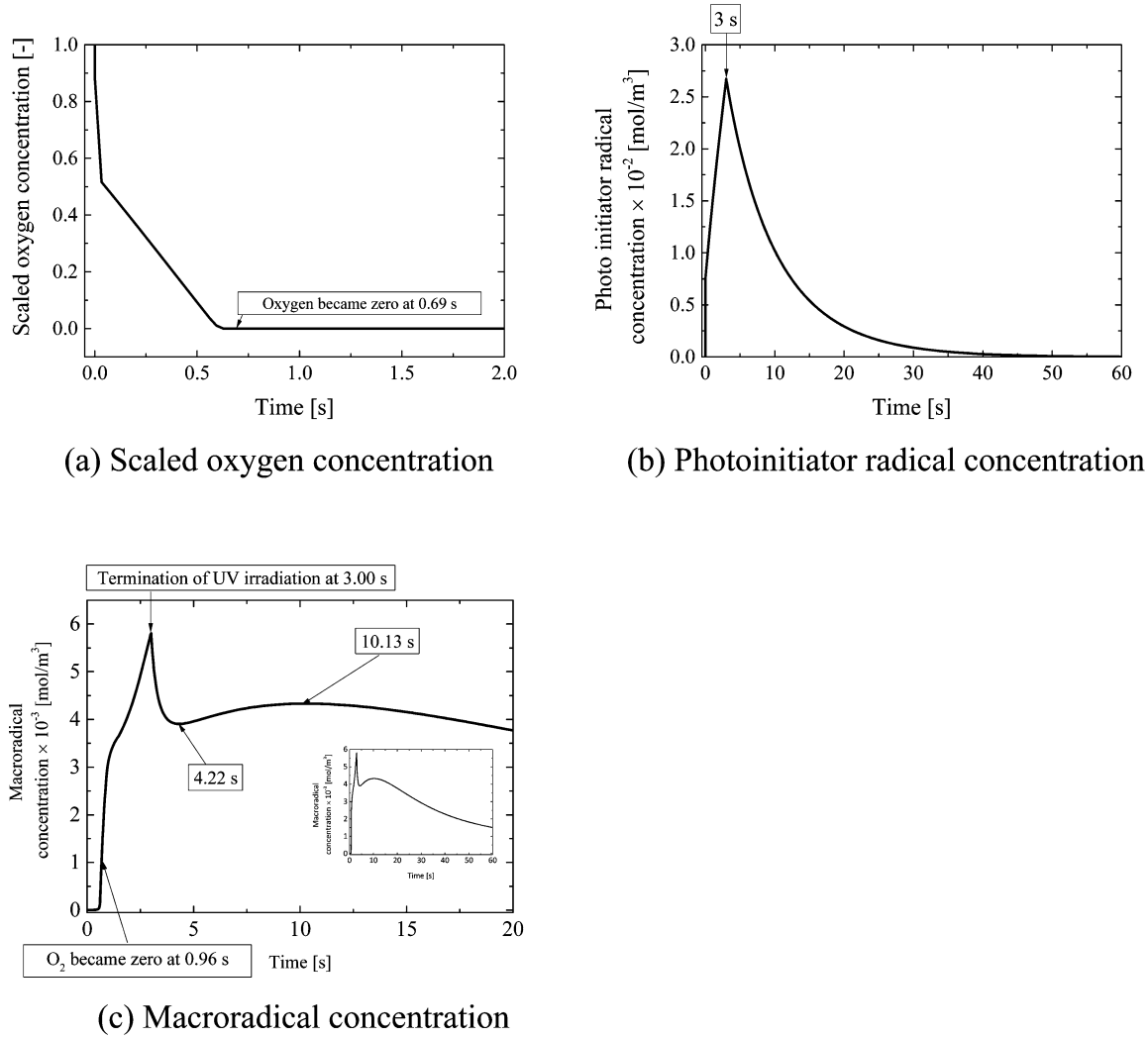

Figure 5. Changes in the (a) oxygen, (b) photoinitiator radical, and (c) macroradical concentrations with time. The inset graph in part c shows the full time scale of change for the macroradical concentration.

conditions. The oxygen-dissolved system was the sample containing oxygen, which inhibits radical polymerization. On the basis of the parameters in Table 2, the results of the numerical simulation were in good agreement with the experimental results and reproduced the change in the methacrylate group conversion. An induction time (oxygen consumption time) preceded the initiation of the radical polymerization. Similar results were obtained by varying oxygen concentration.[44] However, the photopolymerization began without an induction time when the oxygen concentration was set to zero, and the polymerization of the methacrylate group occurred instantaneously. A comparison of these results indicated that the presence of oxygen was an important factor in determining the onset of photopolymerization.

The experimental results indicated that after shutting off the UV light, the polymerization proceeded to a conversion of up to 0.45, as macroradicals and primary radicals were present even after the UV intensity reached 0. The numerical simulation was in good agreement with the postpolymerization results. The mass balance equation for the macroradicals could be used to estimate the macroradical concentration.

Figure 5 presents the scaled oxygen concentration, the photoinitiator radical concentration, and the macroradicals concentration obtained from the numerical simulation after the 3 s irradiation depicted in Figure 4. The oxygen concentration decreased rapidly when the UV irradiation began, followed by a gradual decrease for 0.69 s. Because the rate of reaction between oxygen and the radicals exceeded the propagation rate, the oxygen concentration initially decreased. The concentration of photoinitiator radicals increased during the application of UV irradiation. After terminating the UV irradiation, the photoinitiator concentration decreased with time.

The macroradical concentration rapidly increased after the oxygen concentration fell to nearly zero, until the UV irradiation was terminated. During this period, the primary radicals were supplied by the dissociation of the photoinitiator and reacted with the monomer, which increased the macroradical concentration. The macroradical concentration decreased, then increased, resulting in the formation of a local minimum in the macroradical concentration.

After termination of the UV irradiation, the macroradical concentration decreased because the photoinitiator was no longer dissociated. Then, primary radicals reacted with monomers to form macroradicals, thereby increasing the macroradical concentration. However, the macroradical concentration again decreased due to the limited number of photoinitiator radicals and the occurrence of bimolecular termination.

dx.doi.org/10.1021/ma402437q | *Macromolecules* 2014, 47, 1906−1913

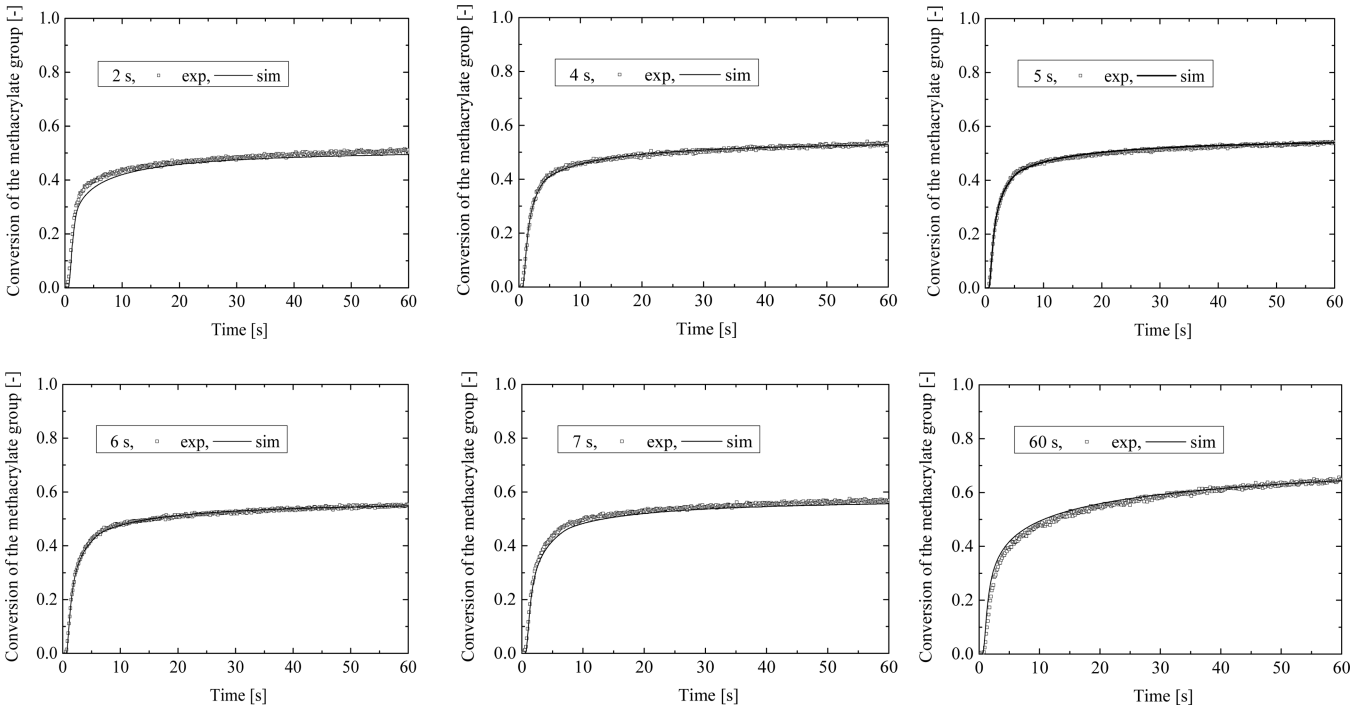

Figure 6. Change in the methacrylate group conversion with different UV irradiation times. The UV intensity was 10 mW·cm^{-2}.

On the basis of eq 5 in Table 1, the macroradical concentration decreased with $k_i[I^\bullet][M]$ due to the decrease in $[I^\bullet]$. The bimolecular termination term $k_t[M_n^\bullet]^2$ decreased simultaneously with the macroradical concentration. When the macroradical concentration increased between 4.22 and 10.13 s, $k_i[I^\bullet][M]$ exceeded $k_t[M_n^\bullet]^2$. Eventually, the value of $k_t[M_n^\bullet]^2$ surpassed that of $k_i[I^\bullet][M]$. The macroradical concentration decreased continuously.

Figure 6 presents the series of methacrylate group conversions with different irradiation times. The conversion at the termination of UV irradiation and the final methacrylate group conversion increased with increased irradiation time. As indicated in the figure, the methacrylate group conversions calculated using the developed model are in good agreement with the experimental data. The reaction rate and the change in conversion after the termination of UV irradiation were used to calculate the kinetic constants for propagation and termination.

Figure 7 provides the kinetic constants obtained from a series of numerical simulations performed in the same manner as those performed for the experiments in which the oxygen concentrations were set to 1.3×10^{-2} mol m^{-3} and zero. The kinetic constants obtained from the simulation in which the oxygen concentration was set to zero decreased monotonically with the conversion. The experimental and simulation results differed significantly up to a conversion of 0.15, with more prominent disparities at low conversion. The kinetic constants obtained from the results involving dissolved oxygen are in good agreement with the conversion experiments.

These results indicate that oxygen exerts a significant effect at low conversions. Few previous studies have reported a peak in the change in the kinetic constant because the specimens were carefully purged to remove any oxygen prior to measurement. For the real-time FT-IR measurements, removing the oxygen from our optical bench proved difficult. Thus, a peak appeared at low conversion values. Although eqs 13 and 14 do not involve any oxygen effect, they work well if the reaction-diffusion equation for oxygen is employed.

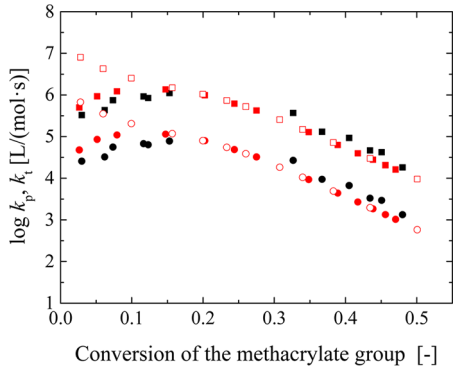

Figure 7. Simulation results for the kinetic constants of propagation and termination. The experimental results for k_p and k_t are denoted with ● and ■, respectively. The simulation results for k_p and k_t are denoted with red ● and red ■ with oxygen and red ○ and red □ without oxygen, respectively.

■ CONCLUSIONS

The effects of dissolved oxygen on the kinetic constants of propagation and termination were investigated via real-time FT-IR measurements and numerical simulations. Oxygen decreased the kinetic constants at low conversions. The effect of oxygen can be modeled by the reaction−diffusion equation for oxygen and the Anseth−Bowman model. The macroradical balancing equation enabled us to simulate the dark polymerization kinetics after terminating UV irradiation and estimate the macroradical concentration. The kinetic constants of the propagation and termination reactions obtained from the numerical simulation of the dark polymerization were in good agreement with the experimental results. The developed model is promising for use in oxygen-dissolved systems, e.g., in roll-to-

dx.doi.org/10.1021/ma402437q | Macromolecules 2014, 47, 1906−1913

roll UV nanoimprint lithography and 3D additive production systems, where the oxygen in air can contact and/or dissolve in UV curable monomers.

AUTHOR INFORMATION

Corresponding Author

*(K.T.)Telephone: +81-238-26-3061. Fax: +81-238-26-3061. E-mail: ktaki@yz.yamagata-u.ac.jp.

Notes

The authors declare no competing financial interest.

ACKNOWLEDGMENTS

This project was financially supported by the New Energy Development Organization (NEDO) (Grant number: 09A16003d), Japan.

REFERENCES

(1) Kloosterboer, J. Network formation by chain crosslinking photopolymerization and its applications in electronics. In *Electronic Applications*: Springer: Berlin and Heidelberg, Germany, 1988; Vol. *84*, pp 1−61.

(2) Yagci, Y.; Jockusch, S.; Turro, N. J. *Macromolecules* **2010**, *43* (15), 6245−6260.

(3) Fouassier, J.-P.; Laevee, J. *Photoinitiators for Polymer Synthesis -Scope, Reactivity, and Efficiency*; Wiley-VCH Verlag & Co. KGaA: Weinheim, Germany, 2012.

(4) Ligon, S. C.; Husár, B.; Wutzel, H.; Holman, R.; Liska, R. *Chem. Rev.* **2013**, *114* (1), 557−589.

(5) Andrzejewska, E. *Prog. Polym. Sci.* **2001**, *26* (4), 605−665.

(6) Krongauz, V. V. *Processes in Photoreactive Polymers*; Chapman & Hall: London, 1995; p 409.

(7) Reiser, A. *Photoreactive Polymers—The Scientific and Technology of Resists*. Wiley-Interscience: New York, 1989; p 409.

(8) Hanrahan, M. J. *RadTech Rep.* **1990**, *4*, 14.

(9) Hoyle, C.; Cole, M.; Kuang, W.; Jonsson, S.; Nason, C.; Ishijima, T.; Kess, R.; Viswanathan, K.; Lee, T. Y.; Ng, R.; Miller, R. *RadTech Rep*, **2002**, *16*, 47.

(10) Bhanu, V. A.; Kishore, K. *Chem. Rev.* **1991**, *91*, 99.

(11) Hoyle, C. E. Presented at UV & EB Technology Expo and Conference, Charlotte, May 2−5, 2004; Charlotte, NC, 2004; p 892.

(12) Benkhoff, J.; Diehliker, K.; Jung, T.; Powell, K.; Sitzmann, E. Presented at RadTech Europe 05, Barcelona, Spain, October 18−20, 2005; Barcelona, Spain, 2005; p 297.

(13) Yoshikawa, H.; Taniguchi, J.; Tazaki, G.; Zento, T. *Microelectron. Eng.* **2013**, *112* (0), 273−277.

(14) Ahn, S. H.; Guo, L. J. *Adv. Mater.* **2008**, *20* (11), 2044−2049.

(15) Ahn, S. H.; Guo, L. J. *ACS Nano* **2009**, *3* (8), 2304−2310.

(16) Schift, H. *J. Vac. Technol. B* **2008**, *26* (2), 458−480.

(17) Dumond, J. J.; Low, H. Y. *J. Vac. Sci. Technol. B* **2012**, *30* (1), 010801−1−28.

(18) Pozzato, A.; Zilio, S. D.; Fois, G.; Vendramin, D.; Mistura, G.; Belotti, M.; Chen, Y.; Natali, M. *Microelectron. Eng.* **2006**, *83* (4−9), 884−888.

(19) Dickey, M. D.; Burns, R. L.; Kim, E. K.; Johnson, S. C.; Stacey, N. A.; Willson, C. G. *AIChE J.* **2005**, *51* (9), 2547−2555.

(20) Berchtold, K. A.; Lovell, L. G.; Nie, J.; Hacioglu, B.; Bowman, C. N. *Polymer* **2001**, *42* (11), 4925−4929.

(21) Berchtold, K. A.; Hacioglu, B.; Lovell, L.; Nie, J.; Bowman, C. N. *Macromolecules* **2001**, *34* (15), 5103−5111.

(22) Kloosterboer, J. G.; Lijten, G. F. C. M.; Greidanus, F. J. A. M. *Polym. Commun.* **1986**, *27*, 268.

(23) Krongauz, V. V.; Yohannan, R. M. *Polymer* **1990**, *31* (6), 1130.

(24) Kongrauz, V. V.; Schmelzer, E. R.; Yohannan, R. M. *Polymer* **1991**, *32* (9), 1654−1662.

(25) Krongauz, V. V.; Schmelzer, E. R. *Polymer* **1992**, *33* (9), 1893−1901.

(26) Dendukuri, D.; Panda, P.; Haghgooie, R.; Kim, J. M.; Hatton, T. A.; Doyle, P. S. *Macromolecules* **2008**, *41* (22), 8547−8556.

(27) Lovestead, T. M.; O'Brien, A. K.; Bowman, C. N. *J. Photochem. Photobiol. A* **2003**, *159* (2), 135−143.

(28) O'Brien, A. K.; Bowman, C. N. *Macromolecules* **2003**, *36* (20), 7777−7782.

(29) Lovestead, T. M.; O'Brien, A. K.; Bowman, C. N. *J. Photochem. Photobiol. A* **2003**, *159* (2), 135−143.

(30) Lovestead, T. M.; Bowman, C. N. *Macromolecules* **2005**, *38* (11), 4913−4918.

(31) Lovestead, T. M.; Berchtold, K. A.; Bowman, C. N. *Macromolecules* **2005**, *38* (15), 6374−6381.

(32) Berchtold, K. A.; Lovestead, T. M.; Bowman, C. N. *Macromolecules* **2002**, *35* (21), 7968−7975.

(33) Goodner, M. D.; Lee, H. R.; Bowman, C. N. *Ind. Eng. Chem. Res.* **1997**, *36* (4), 1247−1252.

(34) Goodner, M. D.; Bowman, C. N. *Macromolecules* **1999**, *32* (20), 6552−6559.

(35) Goodner, M. D.; Bowman, C. N. *Chem. Eng. Sci.* **2002**, *57* (5), 887−900.

(36) Jariwala, A. S.; Ding, F.; Boddapati, A.; Breedveld, V.; Grover, M. A.; Henderson, C. L.; Rosen, D. W. Modeling effects of oxygen inhibition in mask-based stereolithography. *Rapid Prototyping J.* **2011**, *17*, 168−175.

(37) Zhang, Y.; Kranbuehl, D. E.; Sautereau, H.; Seytre, G.; Dupuy, J. *Macromolecules* **2009**, *42* (1), 203−210.

(38) Bowman, C. N.; Peppas, N. A. *Macromolecules* **1991**, *24* (8), 1914−1920.

(39) Anseth, K. S.; Bowman, C. N. *Polym. React. Eng.* **1992−93**, *1* (4), 499−520.

(40) Kurdikar, D. L.; Peppas, N. A. *Macromolecules* **1994**, *27*, 4084−4092.

(41) Anseth, K. S.; Wang, C. M.; Bowman, C. N. *Macromolecules* **1994**, *27* (3), 650−655.

(42) Odian, G. *Principles of Polymerization*; Wiley & Sons: New York, 1991.

(43) Rabek, J. F. Experimental and analytical methods for the investigation of radiation curing. In *Radiation Curing in Polymer Science and Technology*; Elsevier: London, 1993; Vol. *1*, p 329.

(44) O'Brien, A. K.; Bowman, C. N. *Macromolecules* **2006**, *39* (7), 2501−2506.

(45) O'Brien, A. K.; Bowman, C. N. *Macromol. Theory Simul.* **2006**, *15* (2), 176−182.

(46) O'Brien, A. K.; Cramer, N. B.; Bowman, C. N. *J. Polym. Sci., Part A: Polym. Chem.* **2006**, *44* (6), 2007−2014.

(47) Cramer, N. B.; O'Brien, C. P.; Bowman, C. N. *Polymer* **2008**, *49* (22), 4756−4761.

(48) Biswal, D.; Hilt, J. Z. *Macromolecules* **2009**, *42* (4), 973−979.

(49) Taki, K.; Nakamura, T. *J. Cosmetics, Dermatological Sci. Appl.* **2011**, *1* (4), 111−118.

(50) Anseth, K. S.; Wang, C. M.; Bowman, C. N. *Polymer* **1994**, *35* (15), 3243−3250.

(51) Decker, C.; Moussa, K. *Macromolecules* **1989**, *22*, 4455−4462.

(52) Taki, K.; Okumura, S. *Macromolecules* **2010**, *43* (23), 9899−9907.